Available online at www.sciencedirect.com
SCIENCE DIRECT
Sensors and Actuators A 125 (2006) 438–445
SENSORS AND ACTUATORS A PHYSICAL
www.elsevier.com/locate/sna

Design, fabrication, and testing of a 3-DOF HARM micromanipulator on (1 1 1) silicon substrate

Heng-Chung Chang, Julius Ming-Lin Tsai, Hsin-Chang Tsai, Weileun Fang *

Power Mechanical Engineering Department, National Tsing Hua University, Hsinchu 300, Taiwan, ROC

Received 29 December 2004; received in revised form 27 April 2005; accepted 16 June 2005
Available online 9 August 2005

Abstract

In this study, a novel HARM (high aspect ratio micromachining) micromanipulator fabricated on (1 1 1) silicon wafer is reported. The micromanipulator consists of a positioning stage, a robot arm, supporting platforms, conducting wires, and bonding pads. These components are monolithically integrated on a chip through the presented processes. The three-degrees-of-freedom (3-DOF) positioning of the micromanipulator is realized by using the integration of two linear comb actuators and a vertical comb actuator. The robot arm is used to manipulate samples with dimension in the order of several microns to several hundred microns, for instance, optical fibers and biological samples. The robot arm could be a gripper, a needle, a probe, or even a pipette. Since the micromanipulator is made of single crystal silicon, it has superior mechanical properties. A micro gripper has also been successfully designed and fabricated.

Keywords: Micromanipulator; Micro robot arm; Micro gripper; 3-DOF; (1 1 1)Wafer

1. Introduction

According to the characteristic of length scale, the micromanipulator is regarded as one of the promising tools for nano-technology and biological applications. In general, the micromanipulator has components in micron scale feature sizes, and can handle objects ranging from sub-micron to hundred microns size, for instance, the nano-particles and cells. Many different micromanipulators have been reported; for instance, the micro gripper (or named micro tweezers) [1–6], the micro probe [7,8], etc. The thin film micro grippers presented in Refs. [1–3] have demonstrated its application in handling biological sample. The high aspect ratio micromachined (HARM) micro grippers have been realized using SOI substrates [4], Hexsil processes [5], and LIGA technology [6]. The micro probe has successfully been employed for the application of atomic force microscopy [7] and thin film mechanical testing [8]. Presently, commercial micromanipulators fabricated by MEMS technology are also available [9].

The characteristic of the micromanipulator is influenced by its thickness. For instance, the thin film micro grippers have relatively low stiffness in the out-of-plane direction. Thus, it is easy to drive the thin film micro gripper in the out-of-plane direction [2]. However, the unwanted out-of-plane bending deflection of the thin film structure needs to be considered during operation. On the other hand, the HARM micro gripper has a much better stiffness in the out-of-plane direction [4–6], so that it is more difficult for the HARM micro gripper to perform an out-of-plane motion. The performance of the micromanipulator is also limited to its fabrication processes. For instance, it is difficult to integrate the linear comb and vertical comb actuators using the existing fabrication processes. Hence, the existing micromachined manipulator can only move in either in-plane direction or out-of-plane direction. In fact, the thickness as well as stiffness of the micromanipulator is also limited to the fabrication process.

* Corresponding author. Tel.: +886 3574 2923; fax: +886 3573 9372.
E-mail address: fang@pme.nthu.edu.tw (W. Fang).

0924-4247/$ – see front matter © 2005 Published by Elsevier B.V.
doi:10.1016/j.sna.2005.06.013

This study presents a novel stiff HARM micromanipulator which can move with three-degrees-of-freedom (3-DOF). This micromanipulator monolithically integrates linear springs, torsional springs, linear comb actuators, and vertical comb actuators on (1 1 1) silicon substrate. Thus, the in-plane as well as out-of-plane motions of micromanipulator become available. In application, a micro gripper was successfully demonstrated.

2. Design

As shown in Fig. 1, the typical micromanipulator presented in this study consists of supporting platforms, positioning stages, the robot arm, conducting wires, and bonding pads. The supporting platforms and bonding pads as indicated by black color were anchored to the substrate. The rest of the components were freely suspended on top of the silicon substrate, and were supported by the platforms and pads. The micromanipulator is designed to have three degrees of freedom (3-DOF) resulted from three positioning stages which are indicated by gray, slash, and dot patterns, respectively. The positioning stages and supporting platforms were connected to each other by using linear springs (spring #1 and #2) and torsional springs (spring #3). The position of the stages was precisely tuned using linear and vertical comb actuators. The conducting wires to transmit power and signal from pads to actuators were designed to free suspended on top of *Si* substrate. The robot arm illustrated in Fig. 1 is a gripper, however, a needle, a probe, and

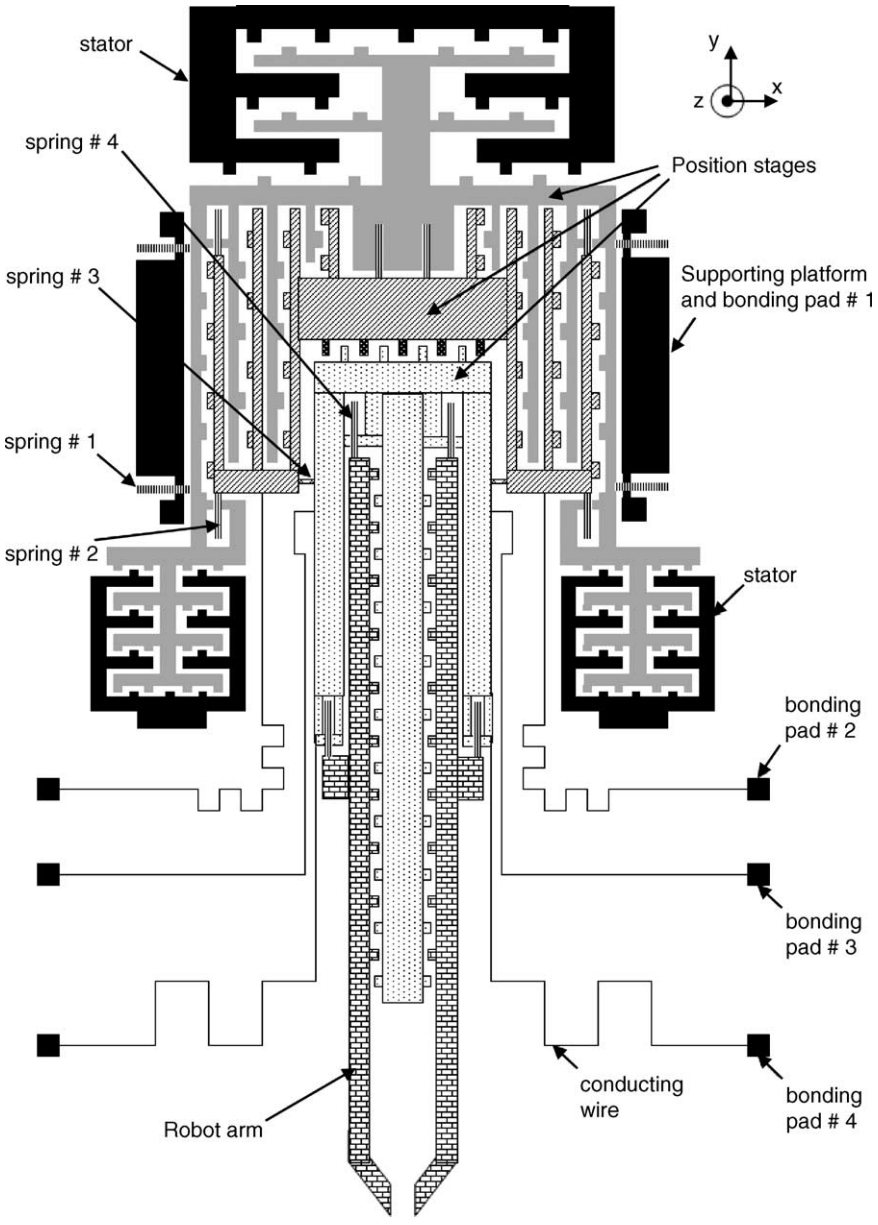

Fig. 1. Schematic illustration of the present 3-DOF micromanipulator.

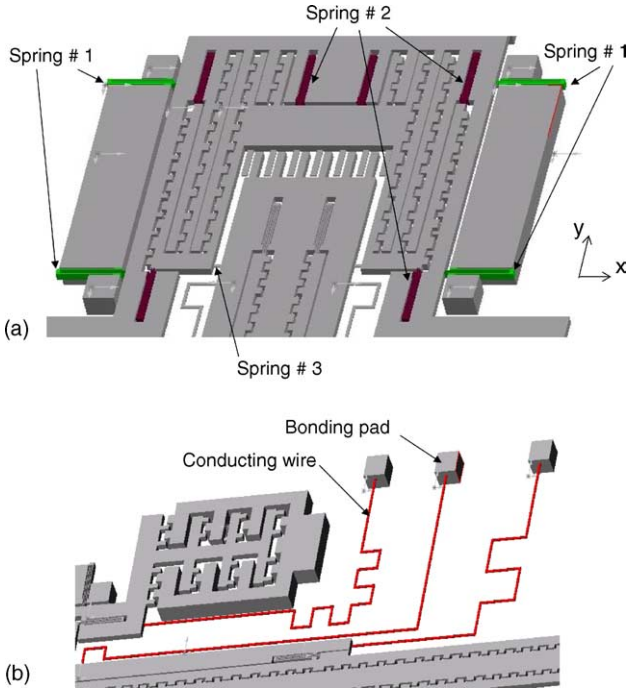

Fig. 2. Close-up illustrations of (a) the three different springs, and (b) the conducting wire and bonding pad.

even a pipette are also available for different applications. The design of the present micromanipulator is detailed as follows.

2.1. The y-direction (in-plane motion) positioning stage

The gray region depicts the *y*-direction positioning stage connecting to the supporting platform (in black pattern) by four linear springs (spring #1). Fig. 2a illustrates the close-up view of the springs. The spring #1 was designed to be flexible only in *y*-direction. The stators indicated in Fig. 1 are anchored to the substrate. The comb electrodes on stators and gray stage formed the *y*-direction comb actuators. Thus, the gray stage will move linearly in the *y*-direction after a driving voltage is input through bonding pad #1.

2.2. The x-direction (in-plane motion) positioning stage

The slash region shows the *x*-direction positioning stage which is connected to the gray stage by six linear springs (spring #2). Fig. 2a illustrates the close-up view of the springs. Spring #2 was flexible only in *x*-direction. The comb electrodes on slash stage and gray stage formed the *x*-direction comb actuators. Thus, the slash stage moved linearly in the *x*-direction after a driving voltage was input through bonding pad #2. Fig. 2b depicts the close-up view of the thin suspended conducting wire and the thick bonding pad. The wire was used to conduct the input signal from bonding pad to stage. The wire was designed to be flexible to prevent the motion of stages from being constrained.

2.3. The z-direction (out-of-plane motion) positioning stage

The dot region indicates the *z*-direction positioning stage which is connected to the slash stage by two torsional springs (spring #3). Fig. 2a also illustrates the close-up view of the springs. Spring #3 was designed to allow the dot stage to rotate out-of-plane. The electrodes between the dot and slash stages were vertical comb type, and the driving voltage was input from bonding pad #3.

2.4. The robot arm

Moreover, the brick region represents the robot arms of micro gripper. As shown in Fig. 1, two robot arms were individually connected to the dot stage using four springs. Similarly, the electrodes on robot arms and dot stage formed the comb actuators. The gap between these two robot arms was adjusted by the electrostatic force and the spring restoring force. Bonding pad #4 was used to input the driving voltage for the gripper.

The micromanipulator has been implemented on the (1 1 1) silicon wafer. Since the micromanipulator was made of single crystal silicon, it has superior mechanical properties than polycrystal and amorphous films. The BELST II process has been employed to realize the present design [10,11], so that the thickness of the micromanipulator can range from several microns to hundred microns. In addition, the thickness of the structure at some particular regions could be trimmed by the BELST II process. Thus, the micromanipulator possessed a thick and stiff robot arm yet it had thin flexible torsional springs and conducting wires. The vertical comb actuator with electrodes located at different vertical position was also monolithically fabricated and integrated. Moreover, the fabrication process to remove the substrate underneath the robot arm has been developed. The robot arm will not be interfered by the substrate during positioning or operation.

3. Fabrication and results

The present micro robot arm has been successfully fabricated using a HARM processes (BELST II process), as illustrated in Fig. 3 [10,11]. The process flow to fabricate the presented micromanipulator is illustrated in Fig. 3. The process began with the boron diffusion on n-type (1 1 1) silicon wafer. After patterned by photolithography, the deep reactive ion etching (DRIE) was employed to create trenches, as shown in Fig. 3a. These trenches were refilled by the following silicon nitride (SiN_x) layer deposition, as shown in Fig. 3b. The present design applied the SiN_x film to provide the electrical isolation for different regions during operation. However, these regions were still mechanically connected with each other through the SiN_x film. Moreover, the trench depth h_t defined by the DRIE process was larger than the

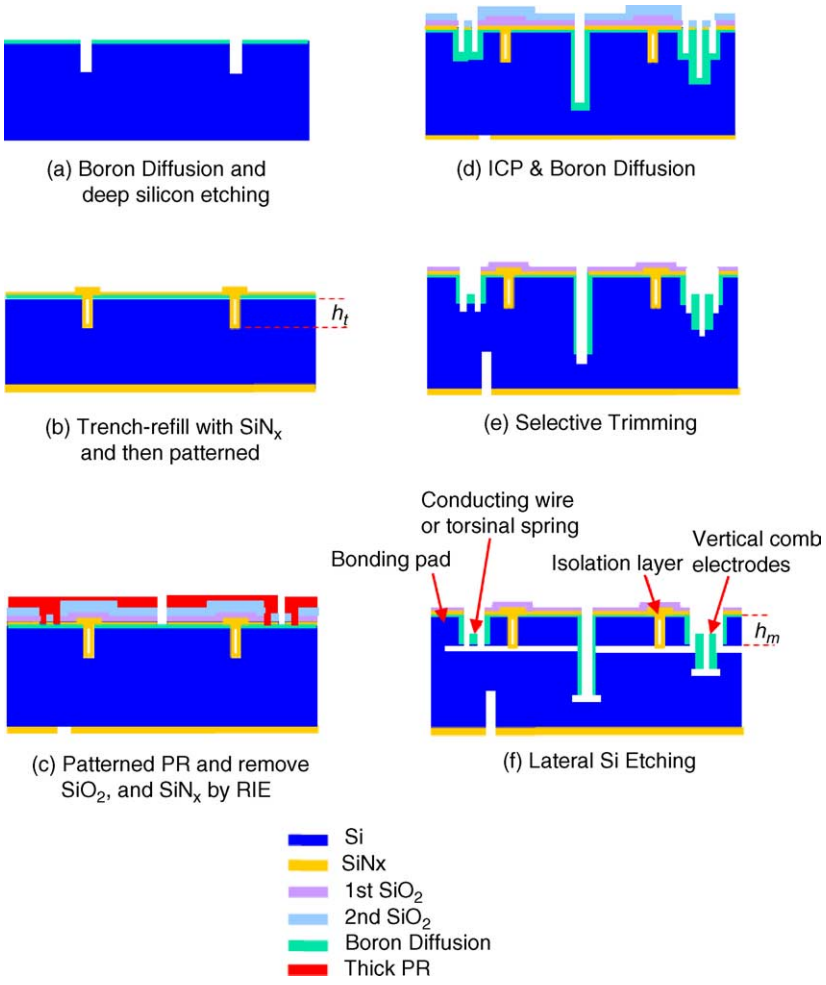

Fig. 3. The fabrication process steps.

thickness of the micromanipulator, h_m, so as to ensure the electrical isolation. The first SiO_2 layer was then deposited by plasma enhanced chemical vapor deposition (PECVD) and patterned with buffered oxide etcher. After that, the second SiO_2 layer was deposited on the substrate. As shown in Fig. 3c, the SiN_x and the two SiO_2 layers were patterned by the RIE and the photolithography processes. The first SiO_2 layer served as the trimming mask (in Fig. 3e) to define the structures to be trimmed including the vertical comb electrode, the torsional suspension, and the conducting wire. The thick photo resist in Fig. 3c is used to define locations of the post to anchor the components, such as stationary comb electrodes and bonding pads. Thus, the three etching masks are properly defined in Fig. 3a–c. Two DRIE processes were used to etch trenches of different depth on the substrate, as shown in Fig. 3d. The first DRIE defined the position anchored to the substrate. The second DRIE defined the thickness of the components, h_m. After that, the boron diffusion was then conducted to provide sidewall-boron diffusion, as illustrated in Fig. 3d. This boron-doped silicon was exploited not only to prevent the sidewall from etching in alkaline solution but also to serve as conducting layer and p–n–p junction insulation. The third DRIE was employed to selectively trim the thickness as well as the vertical position of the components. As shown in Fig. 3e, the height of the stationary electrodes was tuned to offer a better initial engagement between the electrodes. Moreover, the thickness of the torsion suspension was decreased in this step to reduce the driving voltage. However, the thickness and stiffness of stiff structure, such as the robot arm, remained unchanged. Finally, the micromanipulator was released in alkaline solution after an anisotropic lateral etching shown in Fig. 3f.

Meanwhile, the SiN_x film on the backside of the wafer is also patterned in Fig. 3c. The pattern of SiN_x film at the backside of Si substrate was used to define the path of the following dicing process. As shown in Fig. 3e, the substrate was diced along the path on the patterned SiN_x film at the backside of Si. The dicing process was exploited to not only separate the chip of robot arm with the substrate, but also expose the tip of the robot arm. Finally, the movable structures of the micromanipulator were released from the substrate

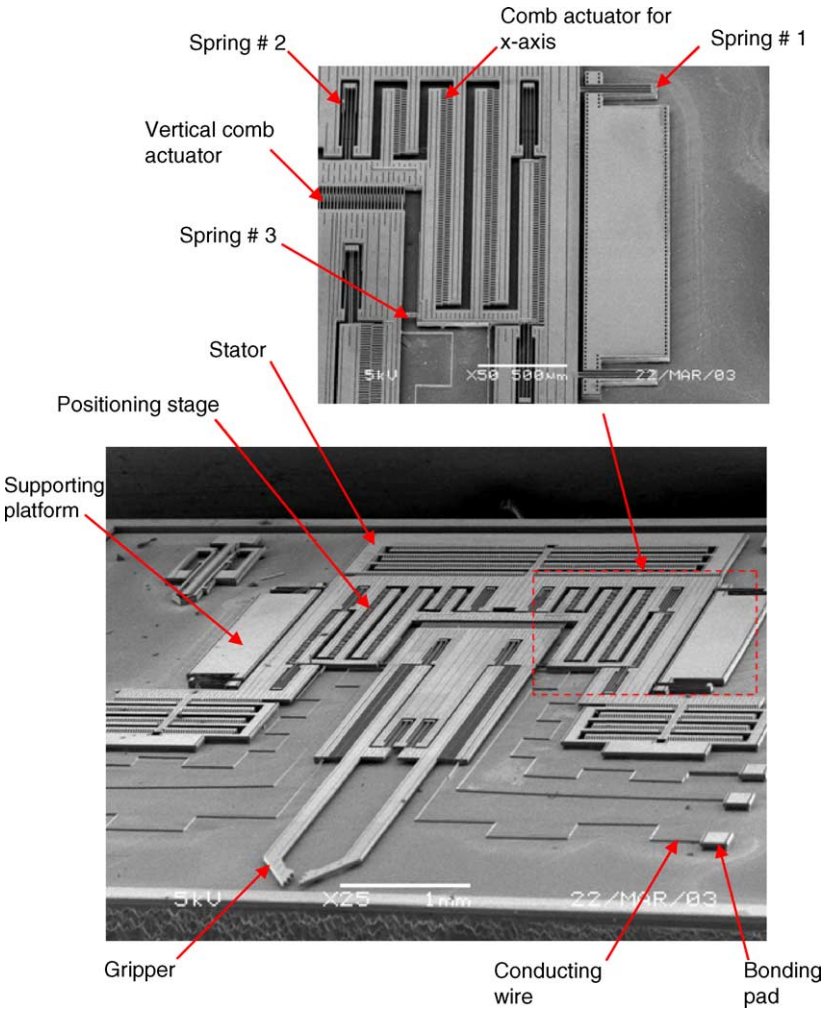

Fig. 4. SEM photo of the fabricated 3-DOF micromanipulator.

after the lateral bulk anisotropic etching of the (1 1 1) Si, as shown in Fig. 3f.

The micro gripper presented in Section 2 was successfully fabricated using the processes in Fig. 3 to demonstrate the feasibility of this study. The SEM photos in Fig. 4 clearly show the fabricated micromanipulator, including supporting platforms, the positioning stage, the robot arm, conducting wires, and bonding pads. Moreover, two linear comb actuators and a vertical comb actuator were successfully integrated on the positioning stage. The close-up SEM photo of the dashed region in Fig. 4 shows three different springs and two different comb actuators. These components were all made of

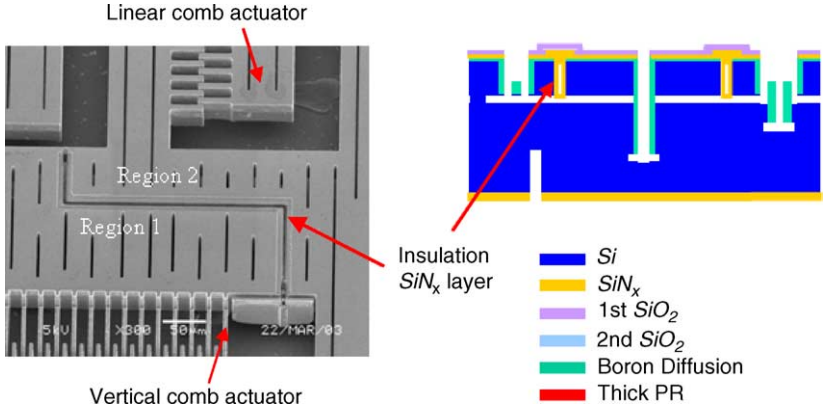

Fig. 5. Close-up view of the insulation layer of the micromanipulator.

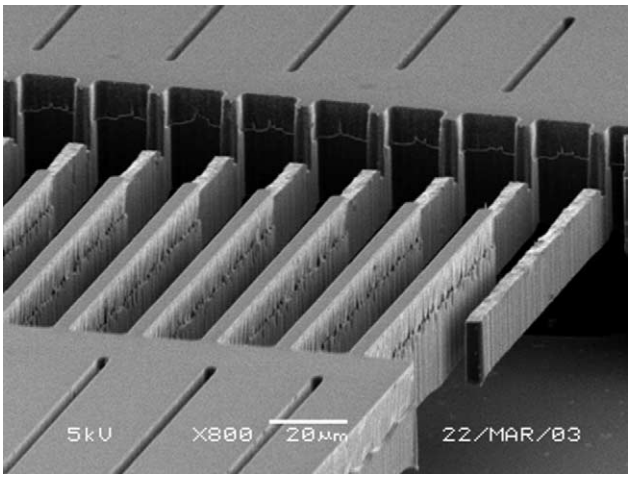

Fig. 6. Close-up view of the vertical comb actuator.

single crystal silicon. In Fig. 4, the conducting wires and torsional springs were 11 μm thick after being trimmed by the process in Fig. 3e. The rest of the components were 25 μm thick.

As indicated in Fig. 5, regions 1 and 2 on the positioning stage are electrical isolated by the trench-refilled dielectric SiN_x film. The linear comb actuator and the vertical comb actuator in Fig. 5 will not interfere with each other during operation. However, these two regions were bonded together by the trench-refilled dielectric SiN_x film. Thus, the positioning stage consisted of regions 1 and 2 was regarded as a whole rigid body during operation. The typical fabrication results of vertical comb electrodes are shown in Fig. 6. The initial engagement between the trimmed stationary and the moving comb fingers is observed. These results demonstrate that the operating region of the vertical comb actuator can be tuned by the thickness trimming process in Fig. 3e.

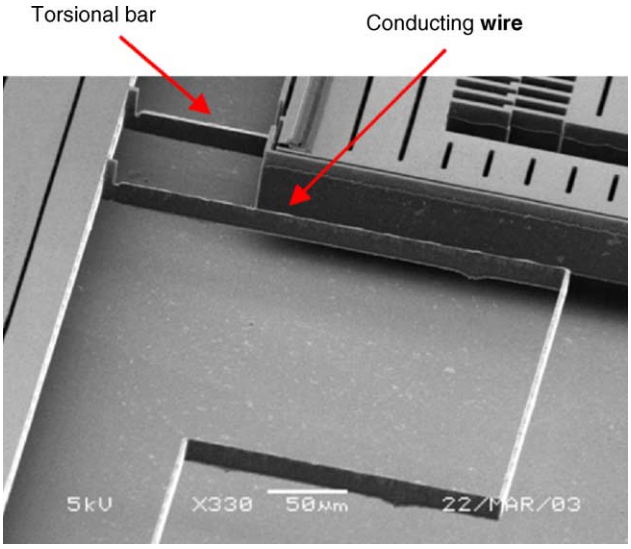

Fig. 7. Close-up view of the trimmed torsional spring and conducting wire.

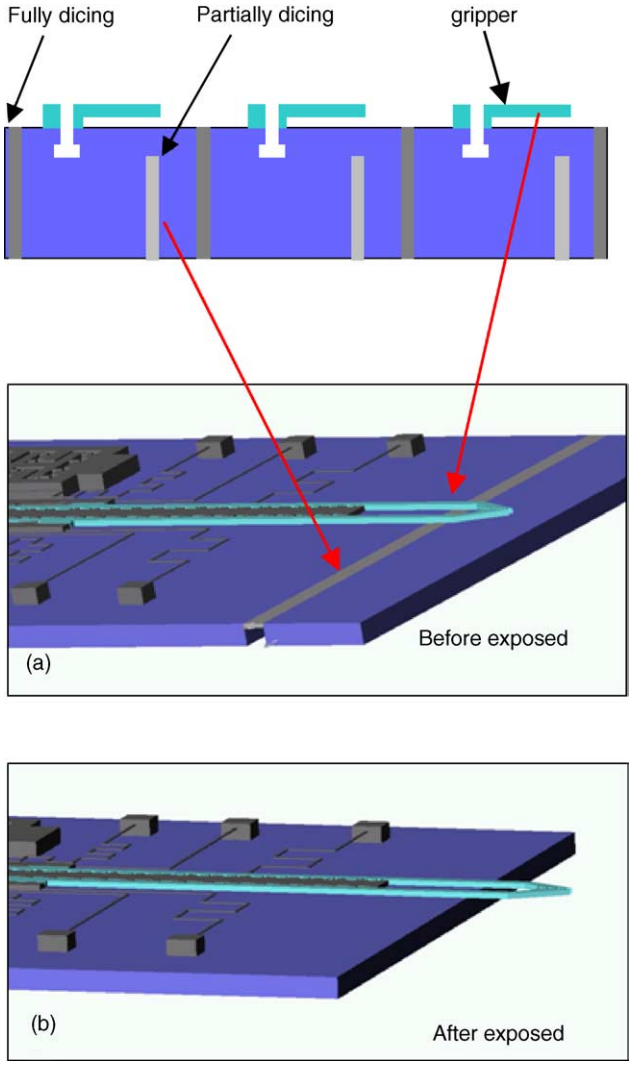

Fig. 8. Schematic illustrations of the approach to expose the gripper head.

Fig. 7 shows the fabrication results of the trimmed suspended conducting wire and torsional spring. The trimmed torsional spring further reveals the capability of the process in Fig. 3 to enable the present micromanipulator to reduce its driving voltage yet maintain the stiffness of its robot arm. This study employed the dicing technique in Fig. 3e to expose the tip of the robot arm. As illustrated in Fig. 8a, the dicing process provided grooves with two different depths on the substrate. One of the grooves was fully through the substrate so as to separate the chip. Whereas, another groove was only 350 μm deep, so that the robot arm remained supported by the substrate underneath during the undercut process in Fig. 3f. After the undercut process, the substrate under the robot arm was removed easily due to the stress concentration effect, as illustrated in Fig. 8b. Thus, the tips of the overhanging gripper arm were allowed to fully exposed after the whole robot arm was released. Fig. 9 shows the SEM photo of a typical result where the tip of the gripper was successfully exposed.

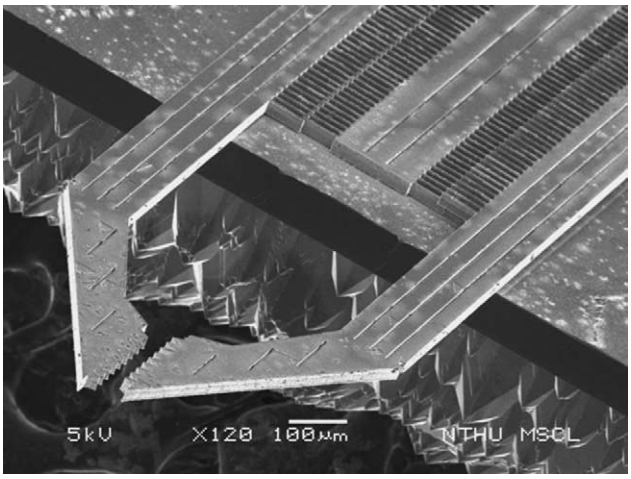

Fig. 9. SEM photo of the exposed gripper head.

4. Testing and results

A test setup was established to characterize the performances of the micromanipulator. In this test setup, a commercialized dynamic test system was employed to drive the micromanipulator first. The test system captured the image of the micromanipulator during operation, so that the in-plane displacement of the micromanipulator was determined. In addition, the out-of-plane displacement of the micromanipulator was measured using a commercial optical interferometer with sub-nanometric resolution. Since the lengths of the robot arm as well as the z-direction positioning stage were known in advance, their angular displacements were also determined.

Firstly, the static load-deflection characteristic of the micromanipulator was determined by the test system. The typical out-of-plane angular displacement of the positioning stage was 0.043° under a 50 V driving voltage. In addition, under a 20 V driving voltage, the in-plane displacement of the positioning stage in both x- and y-directions were 1.03 and 0.85 μm, respectively. The displacement of the gripper was 5.93 μm under a 50 V driving voltage. The gripper has been used to seize various objects. As shown in Fig. 10, the gripper is grasping an ant's leg.

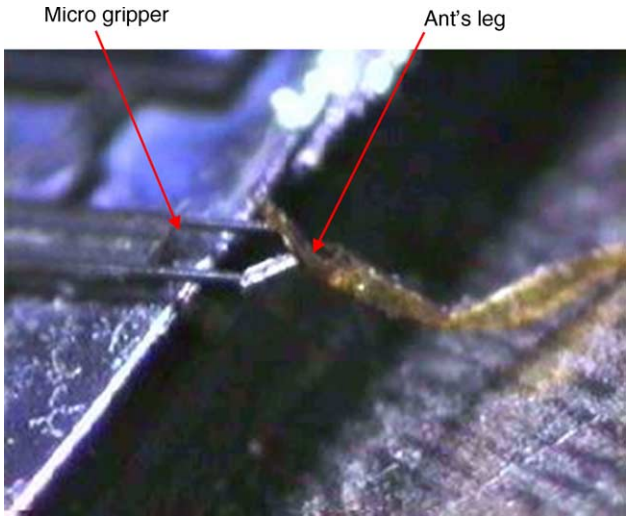

Fig. 10. Manipulation of an ant's leg using the 3D micromanipulator.

5. Conclusions

This study has presented the design and fabrication of a 3-DOF HARM micromanipulator on (1 1 1) silicon wafer. The BELST II process was employed to implement the present micromanipulator. Thus, components of the micromanipulator were monolithically fabricated and integrated on a chip. The 3-DOF positioning of the micromanipulator is realized by using the integration of two linear comb actuators and a vertical comb actuator. Moreover, the micro gripper with two robot arms have also been successfully designed and fabricated for grasping applications. In conclusion, there are four merits of the present micromanipulator: (1) monolithically integrating the vertical comb actuator and linear comb actuators to offer the 3-DOF motions; (2) the micromanipulator can possess a thick and stiff robot arm yet it has thin flexible torsional spring to reduce the driving voltage; (3) the actuators on the same positioning stage can be operated and controlled individually with the aid of the trench-refilled dielectric SiN_x isolation layer; (4) the flexible suspended thin conducting wires are implemented to prevent the wire bonding on suspended components. Moreover, the micromanipulator has superior mechanical properties since it was made of single crystal silicon.

Acknowledgements

This project was (partially) supported by the National Science Council (Taiwan) under contract no. NSC 93-2212-E-007-012. The authors would like to appreciate the National Science Council Central Regional MEMS Research Center (Taiwan), Semiconductor Center of National Chiao-Tung University (Taiwan), and National Nano Device Laboratory (Taiwan) in providing the fabrication facilities.

References

[1] C.J. Kim, A.P. Pisano, R.S. Muller, Silicon-processed overhanging microgripper, J. Microelectromech. Syst. 12 (1992) 31–36.
[2] J. Ok, M. Chu, C.J. Kim, Pneumatically driven microcage for micro-objects in biological liquid, in: IEEE MEMS'99, Orlando, FL, 1999, pp. 459–463.
[3] J.W.L. Zhou, H.Y. Chan, T.K.H. To, W.J. Li, Polymer MEMS actuators for underwater micromanipulation, IEEE-ASME Trans. Mechatronics 9 (2004) 334–342.
[4] B.E. Volland, H. Heerlein, I.W. Rangelow, Electrostatically driven microgripper, Microelectr. Eng. 61–62 (2002) 1015–1023.
[5] R.T. Howe, C.G. Keller, Hexsil tweezers for teleoperated micro-assembly, in: IEEE MEMS'97, Nagoya, Japan, 1997, pp. 72–77.

[6] M.C. Carrozza, A. Menciassi, G. Tiezzi, P. Dario, The development of a LIGA-microfabricated gripper for micromanipulation tasks, J. Micromech. Microeng. 8 (1998) 141–143.
[7] T. Akiyama, U. Staufer, N.F. de Rooji, Atomic force microscopy using an integrated comb-shape electrostatic actuator for high-speed feedback motion, Appl. Phys. Lett. 76 (2000) 3139–3141.
[8] M.A. Haque, M.T.A. Saif, Microscale materials testing using MEMS actuators, J. Microelectromech. Syst. 10 (2001) 146–152.
[9] G. Skidmore, M. Ellis, A. Geisberger, K. Tsui, K. Tuck, R. Saini, T. Udeshi, M. Nolan, R. Stallcup, J. Von Her rII, Assembly technology across multiple length scales from the micro-scale to the nano-scale, in: IEEE MEMS'04, Maastricht, the Netherlands, 2004, pp. 588–592.
[10] J. Hsieh, W. Fang, A boron etch-stop assisted lateral silicon etching process for improved high-aspect-ratio silicon micromachining and its applications, J. Micromech. Microeng. 12 (2002) 574–581.
[11] C.C. Chu, J.M.L. Tsai, J. Hsieh, W. Hsieh, Fang, A novel electrostatic vertical comb actuator fabricated on (1 1 1) silicon wafer, in: IEEE MEMS'03, Kyoto, Japan, 2003, pp. 56–59.

Biographies

Heng-Chung Chang was born in Taichung, Taiwan, in 1979. He received his Master degree from Power Mechanical Engineering Department of National Tsing Hua University in 2003. Currently he is working in research center of Delta Electronics Inc., Taiwan. His current research interests include microstructures design, sensor applications, processes integration.

Julius Ming-Lin Tsai was born in Taipei, Taiwan 1976. He received his B.S. and PhD degree in Power Mechanical Engineering Department, National Tsing Hua University, Taiwan, in 1998 and 2004 respectively. In 2003, he received scholarship program provided by National Science Console and studied with Prof. Gary K. Fedder in Carnegie Mellon University, US. He is currently interested in MEMS applications in optical systems, inertial sensors and micro system modelling.

Hsin-Chang Tsai was born in Chai-Yi, Taiwan, in 1974. He received his B.S. and PhD degree from Power Mechanical Engineering Department of National Tsing Hua University in 1997 and 2003. Currently, he is working in a MEMS research center of Delta Electronics Inc., Taiwan. His current research interests include characterization and modeling of the mechanical properties of thin films, microstructures design and manufacture for thermal management applications.

Weileun Fang was born in Taipei, Taiwan, in 1962. He received his PhD degree from Carnegie Mellon University in 1995. His doctoral research focused on the determining of the mechanical properties of thin films using micromachined structures. In 1995, he worked as a postdoctoral research at Synchrotron Radiation Research Center, Taiwan. He is currently an associate professor at Power Mechanical Engineering Department, National Tsing Hua University, Taiwan. His research interests include MEMS with emphasis on micro optical systems, microactuators and the characterization of the mechanical properties of thin films.